catalysts

MDPI

Article

One-Step Synthesis of $MoS_2/TiSi_2$ via an In Situ Photo-Assisted Reduction Method for Enhanced Photocatalytic H_2 Evolution under Simulated Sunlight Illumination

Chunyong Zhang [1,2], Aijuan Liu [1], Kezhen Li [1], Yukou Du [1] and Ping Yang [1,*]

[1] College of Chemistry, Chemical Engineering and Materials Science, Soochow University, Suzhou 215123, China; zhangcy@jsut.edu.cn (C.Z.); nshi0598@gmail.com (A.L.); nshi058@gmail.com (K.L.); duyk@suda.edu.cn (Y.D.)

[2] Jiangsu Key Laboratory of Precious Metal Chemistry and Technology, Jiangsu University of Technology, Changzhou 213001, China

* Correspondence: pyang@suda.edu.cn; Tel.: +86-512-6588-0089

Received: 11 March 2019; Accepted: 20 March 2019; Published: 25 March 2019

Abstract: A new $MoS_2/TiSi_2$ complex catalyst was designed and synthesized by a simple one-step in situ photo-assisted reduction procedure. The structural and morphological properties of the composites were characterized by X-ray diffraction (XRD), transmission electron microscopy (TEM), scanning electron microscopy (SEM), and ultraviolet-visible diffused reflectance spectroscopy (UV-vis DRS), which proved the formation of $MoS_2/TiSi_2$. $MoS_2/TiSi_2$ with optimized composition showed obviously enhanced photocatalytic activity and superior durability for water reduction to produce H_2. The H_2 generation rate over the $MoS_2/TiSi_2$ photocatalyst containing 3 wt % MoS_2 reached 214.1 $\mu mol \cdot h^{-1} \cdot g^{-1}$ under visible light irradiation, which was ca. 5.6 times that of the pristine $TiSi_2$. The improved photocatalytic activity of $MoS_2/TiSi_2$ could be related to the broad response spectrum, large visible light absorption, and synergies among MoS_2 and $TiSi_2$ that enhance photoexcited charge transfer and separation.

Keywords: $MoS_2/TiSi_2$; in situ synthesis; visible light; hydrogen generation

1. Introduction

In recent decades, semiconductor photocatalysis has received close attention owing to its potential application in the production of renewable hydrogen [1,2]. Since the discovery of photoelectrocatalytic H_2 production in the TiO_2 electrode by Fujishima and Honda in 1972 [3], the semiconductor photocatalyst ($Eg \approx 3.2$ eV) has been investigated extensively [4,5]. However, due to its inherent shortcomings, such as its broad bandgap and low quantum efficiency [6], researchers have been making great efforts to modify TiO_2 or seek novel semiconductor photocatalysts to improve the photocatalytic activity and efficiency [7].

A novel compound material, titanium disilicide ($TiSi_2$) has been attracting interest because of its thermal stability, good electrical conductivities, single electron tunneling characteristics, and eminent light absorption ability from near-UV to visible light (e.g., ~3.4–1.5 eV) [8,9]. Ritterskamp et al. first used $TiSi_2$ as a photocatalyst for water splitting [10]. After that, a series of $TiSi_2$-based compounds or composites, including $TiSi_2$–SiC [11], Ti_5Si_3 [12], $TiO_2/TiSi_2$ [7,8], were synthesized. $RuO_2/TiSi_2$/RGO hybrid and $WS_2/TiSi_2$ composite were also successfully synthesized by our group [1,13]. These novel materials showed improved photoelectrochemical properties and enhanced photocatalytic activity.

In recent years, the indirect-gap semiconductor MoS_2 ($Eg \approx 1.8$ eV) has found many potential uses in the fields of microelectronics, lithium batteries, H_2 storage, and catalysis for hydrodesulphurization. More importantly, composites formed by modifying the primary catalysts with MoS_2, such as MoS_2/CdS [14], MoS_2/grapheme [15], and MoS_2/zinc cadmium sulfide [16], demonstrated improved activity for photocatalytic water splitting to produce hydrogen.

The conduction band (CB) of $TiSi_2$ (−0.43 eV) [10] is higher than that of MoS_2 (−0.1 eV) [17], and the valence band (VB) of $TiSi_2$ (1.07 eV) [10] is lower than that of MoS_2 (1.7 eV) [17]. When $TiSi_2$ and MoS_2 are combined to form a composite photocatalyst, the electrons on the conduction band of $TiSi_2$ can be transferred to the conduction band of MoS_2, and the holes on the valence band of MoS_2 can be transferred to the valence band of $TiSi_2$. The combination of MoS_2 used as co-catalysts and $TiSi_2$ used as main catalysts is probably beneficial to the catalytic performance of hydrogen production. According to our own survey of the literature, MoS_2-functionalized $TiSi_2$ materials have not been reported. Therefore we cover a novel hybrid consisted of MoS_2 and $TiSi_2$ by one-step in situ photo-reduction and its photocatalytic application for the photocatalytic H_2 evolution under visible light.

2. Results and Discussion

2.1. Morphology and Structure

The XRD patterns of MoS_2, $TiSi_2$, and MoS_2-modified $TiSi_2$ composite ($MoS_2/TiSi_2$-3) are shown in Figure 1. The XRD pattern of the measured MoS_2 sample demonstrates peaks located at 13.8°, 32.0°, 39.0°, 57.7°, and 59.6°, which can be indexed to the (002), (100), (103), (110), and (003) hexagonal crystallographic faces of molybdenum disulfide (JCPDS No. 37-1492), respectively. The XRD pattern of $TiSi_2$ displays distinct diffraction peaks at 23.3°, 38.6°, 41.7°, 42.6°, and 49.3°, corresponding to the (111), (311), (040), (022), and (331) planes of face-centered orthorhombic structure of $TiSi_2$ (JCPDS No. 35-0785). From the XRD pattern of $MoS_2/TiSi_2$, the characteristic peaks of $TiSi_2$ and MoS_2 with similar position can be detected after the reaction process, indicating that MoS_2 has been synthesized by photo-reduction.

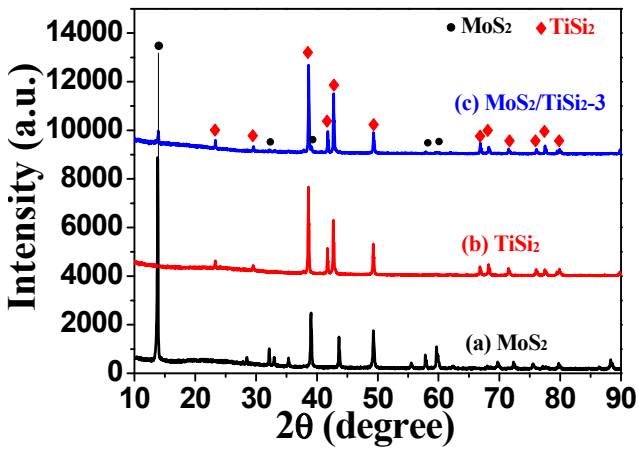

Figure 1. XRD patterns of the MoS_2 (**a**), $TiSi_2$ (**b**), and $MoS_2/TiSi_2$-3 (**c**).

The morphology of $MoS_2/TiSi_2$ was determined by SEM and TEM and demonstrated in Figure 2 and Figure S1. $TiSi_2$ consists of grains of irregular shape with flat surfaces and sharp edges. The size of the grains is in the range of 1–10 μm. MoS_2 particles of about 400 nm are well dispersed at the surface of $TiSi_2$. The EDS results of the $MoS_2/TiSi_2$ sample (Figure S2) reveal that the composite consists of Mo, S, Ti, and Si, further proving that MoS_2 has been successfully deposited at $TiSi_2$.

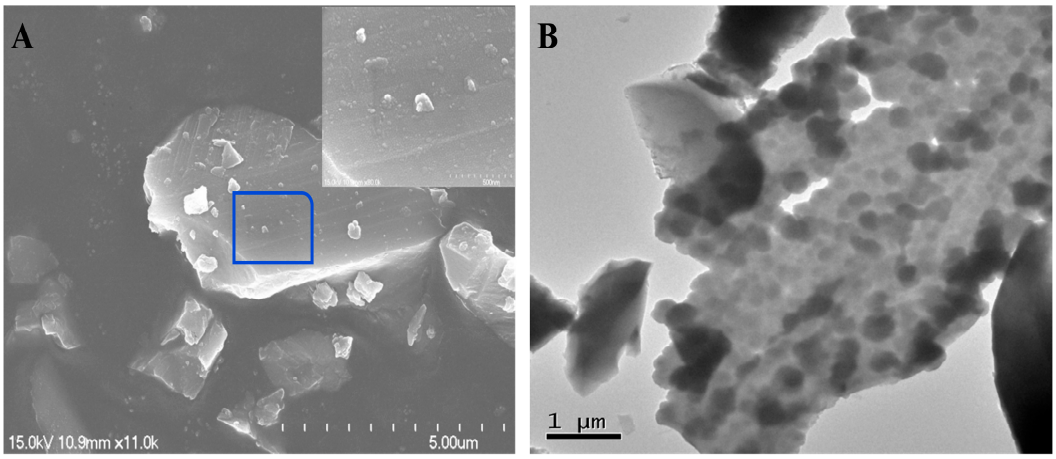

Figure 2. SEM (**A**) and TEM (**B**) images of $MoS_2/TiSi_2$-3.

XPS was carried out and the corresponding results are shown in Figure 3 and Figure S3. Figure 3A shows the high-resolution Ti 2p XPS spectra of the samples. The peaks located at 453.5, 458.9, and 464.8 eV are attributed to Ti^0 $p_{3/2}$, Ti^{4+} $p_{3/2}$, and Ti^{4+} $p_{1/2}$ [10,18], respectively. The peaks located at 98.6 and 102.4 eV in the pattern of $TiSi_2$ (Figure 3B) were attributed to Si^0 $p_{3/2}$ and Si^{4+} $p_{3/2}$ [18,19]. Comparing the above peak positions with those of $MoS_2/TiSi_2$, the binding energy of Ti^{4+} and Si^{4+} in $MoS_2/TiSi_2$-3 is higher than in $TiSi_2$, while the binding energy of Ti^0 and Si^0 in $MoS_2/TiSi_2$-3 is lower than in $TiSi_2$. The peak located at 163.2 eV confirms the presence of S^{2-} in MoS_2 (Figure 3C). The blue shift of the S 2p peak position of $MoS_2/TiSi_2$-3 can be clearly observed. The changes in binding energy of S were possibly due to the S-Ti and S-Si bond formation. The shift of the relative peak position is attributed to the interaction of $TiSi_2$ with MoS_2 [1,18,20]. Figure 3D demonstrates the XPS spectra of Mo 3d for MoS_2 and $MoS_2/TiSi_2$-3. The Mo 3d peak positions of $MoS_2/TiSi_2$-3 also shift to higher binding energies, indicating a low load of MoS_2 and the remarkable combination effect of MoS_2 and $TiSi_2$ [14,21].

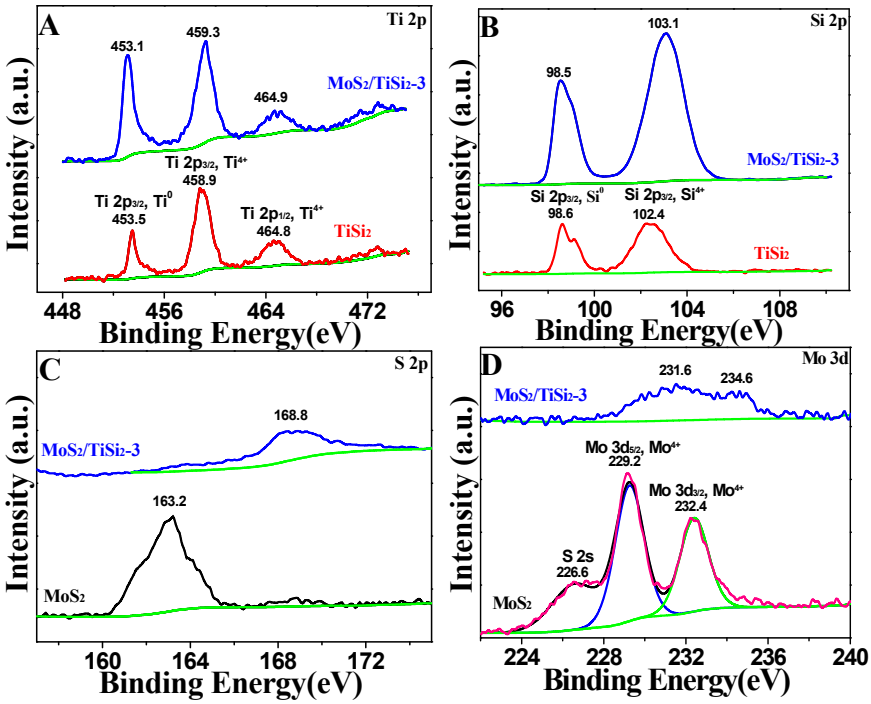

Figure 3. XPS of (**A**) Ti 2p for $TiSi_2$ and $MoS_2/TiSi_2$-3, (**B**) Si 2p for $TiSi_2$ and $MoS_2/TiSi_2$-3, (**C**) S 2p for MoS_2 and $MoS_2/TiSi_2$-3, (**D**) Mo 3d for MoS_2 and $MoS_2/TiSi_2$-3.

2.2. Optical and Photoelectrochemical Properties

Figure 4 exhibits the UV-vis absorption spectra of the obtained samples. The absorption of pure $TiSi_2$ is in the range of ca. 400 up to 850 nm, where its absorption is higher than that of MoS_2. The $MoS_2/TiSi_2$-3 sample demonstrates higher absorption intensity compared with MoS_2 and $TiSi_2$, indicating that the $MoS_2/TiSi_2$ composite possesses enhanced ability for harvesting visible light.

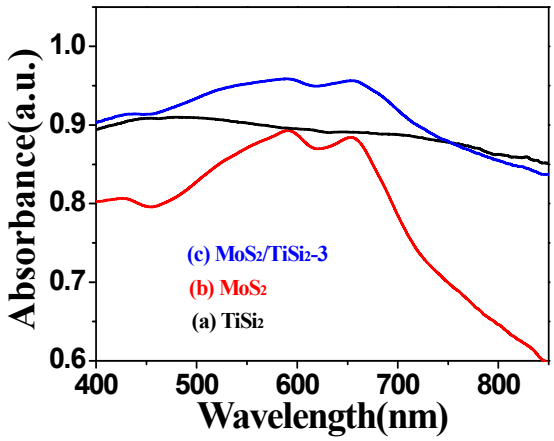

Figure 4. The UV–vis absorption spectra of the obtained samples.

The photocurrent responses for $TiSi_2$, MoS_2, and $MoS_2/TiSi_2$-3 are displayed in Figure 5A. The photocurrent density of $TiSi_2$ or MoS_2 is rather low (ca. 0.22 $\mu A \cdot cm^{-2}$). The photocurrent density of $MoS_2/TiSi_2$-3 (0.59 $\mu A \cdot cm^{-2}$) is more than 2.6 times that of $TiSi_2$ in the same irradiation conditions. The results suggest the positive synergetic effect between MoS_2 and $TiSi_2$, which leads to enhanced photoinduced chargers transfer and separation. Figure 5B shows the electrochemical impedance spectra (EIS) of the samples are shown in. The diameter of the semicircle of $MoS_2/TiSi_2$-3 plot is obviously smaller than that of MoS_2 and $TiSi_2$, which indicates effectively enhanced carrier transfer at the interface between the $MoS_2/TiSi_2$-3 electrode and the electrolyte [22]. The experimental data for all the electrodes can be expressed as an equivalent circuit, displayed as shown as the inset of Figure 5B, in which CPE1 is constant phase elements connected in parallel with R2 [23,24], R2 is the resistance of solution, and the ohmic series resistance (R1) is the resistance of charge-transfer resistance at interfaces [25,26].

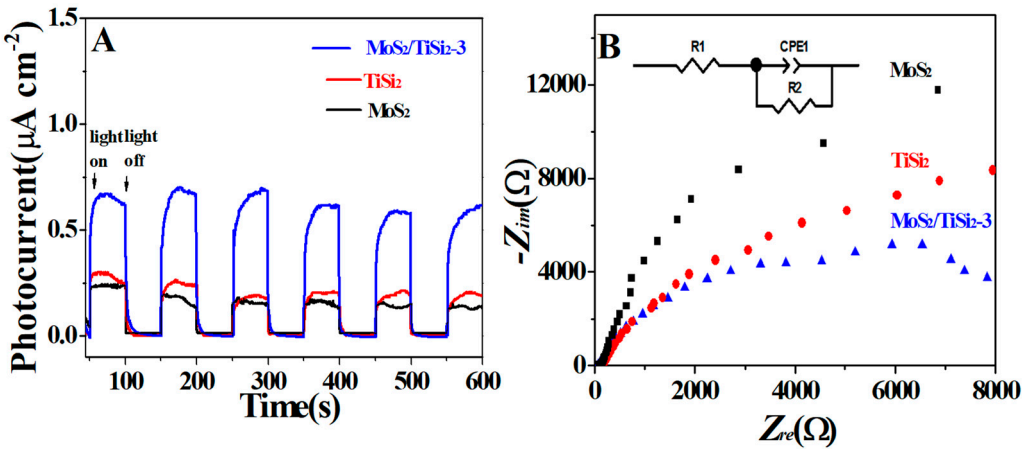

Figure 5. (**A**) The photocurrent responses of samples under 150 W xenon lamp. The electrolyte was 60 mL of 0.5 M Na_2SO_4 solution containing 6 mL lactic acid; (**B**) The electrochemical impedance spectra (EIS) for the samples in 60 mL of 0.5 M Na_2SO_4 solution containing 6 mL lactic acid.

2.3. Photocatalytic Activity

The photocatalytic activity for H_2 production of the samples are shown in Figure 6 and Figure S4. MoS_2 alone shows little photocatalytic activity. The hydrogen production rate for $TiSi_2$ is 38.4 μmol·h^{-1}·g^{-1}. The hydrogen production rate for the $MoS_2/TiSi_2$-1 sample increases to 119.6 μmol·h^{-1}·g^{-1}. The photocatalytic activity of the $MoS_2/TiSi_2$ augments with the increasing of the quantity of MoS_2 in $MoS_2/TiSi_2$. The hydrogen production rate of the $MoS_2/TiSi_2$-3 sample reaches the maximum value 214.1 μmol·h^{-1}·g^{-1}, which is approximately 5.6 times that of $TiSi_2$. The fact that composite catalysts exhibit much enhanced activity for H_2 evolution can be attributed to the synergistic effect between $TiSi_2$ andMoS_2. Through the heterojunction formed between MoS_2 and $TiSi_2$, the photogenerated electrons in $TiSi_2$ easily transfer to the conduction band of MoS_2, which inhibits the recombination of e^--h^+, thus improving the photocatalytic activity.

The results of the stability are shown in Figure 6. In the total 25 h recycle tests, the photocatalytic activity for H_2 production of $MoS_2/TiSi_2$-3 was almost invariable and the average value was 214 μmol·h^{-1}·g^{-1}, indicating that the composite prepared by the in situ photo-assisted reduction of MoS_2 on $TiSi_2$ possesses good photocatalytic stability.

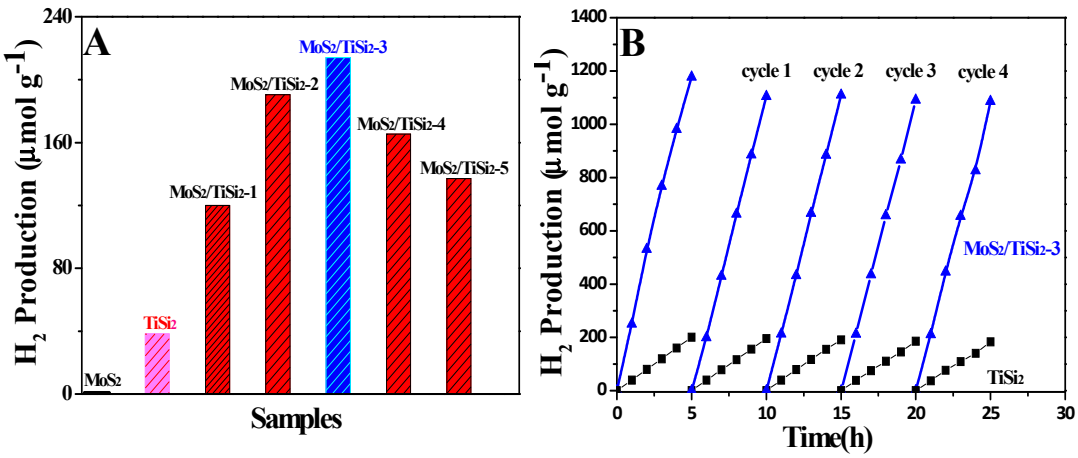

Figure 6. (**A**) The amount of H_2 evolved over the samples and (**B**) cycling measurement.

Because of the wide-bandgap energy (3.4~1.5 eV) for $TiSi_2$, $TiSi_2$ can easily absorb the photons under visible light irradiation to generate plenty of electrons and holes in its conduction and valence band, respectively [8]. Well-combined $MoS_2/TiSi_2$ heterojunctions can prompt the transfer of photogenerated chargers between MoS_2 and $TiSi_2$, and provide a pathway for charges transfer simultaneously (Scheme S1). Since the CB of $TiSi_2$ (−0.43 eV) is more negative than that of MoS_2 (−0.1 eV), the photogenerated electrons in the CB of $TiSi_2$ were easy to transfer through the heterojunction interface between MoS_2 and $TiSi_2$ to the CB of MoS_2 particles deposited on the surface of $TiSi_2$. Simultaneously, the holes transfer from the higher VB of MoS_2 (1.7 eV) to the VB of $TiSi_2$ (1.07 eV). The shorter charge transfer route effectively restrains the recombination process of the electron-hole pairs. H^+ is reduced to hydrogen atom, to form hydrogen by the electrons in the CB of MoS_2, while the holes on the $TiSi_2$ surface are rapidly scavenged by H_2O and OH-, generating ·OH to oxidize sacrificial agents.

2.4. Formation Mechanism of the $MoS_2/TiSi_2$ Photocatalyst

Scheme 1 shows the proposed formation mechanism of the $MoS_2/TiSi_2$ photocatalyst. The electrons are generated at the VB of $TiSi_2$ are excited by visible-light, which in turn reduce $[MoS_4]^{2-}$ to MoS_2 [16], as shown in Equation (1):

$$[MoS_4]^{2-} + 2e \rightarrow MoS_2 + 2S^{2-}. \quad (1)$$

The holes (h) of $TiSi_2$ are scavenged by lactic acid. MoS_2 particles supported on the surface of $TiSi_2$ not only form a heterojunction with $TiSi_2$ but also provide effective active sites to improve hydrogen production.

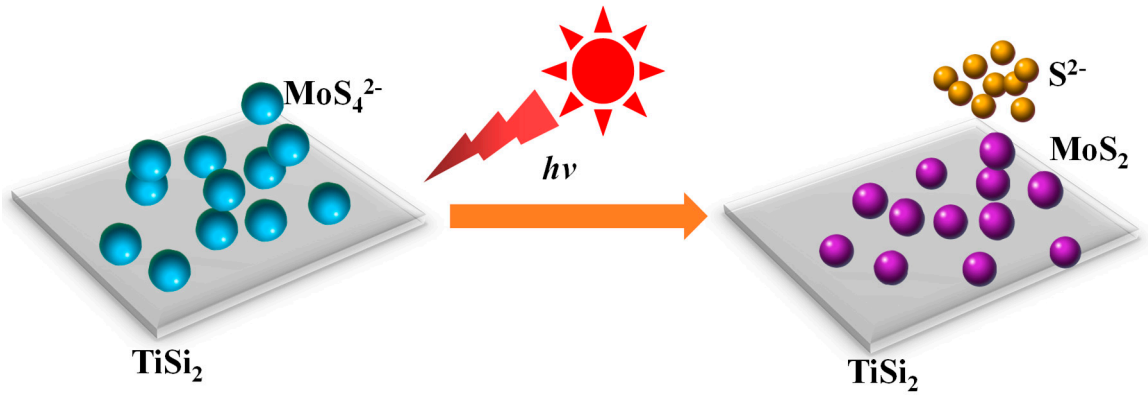

Scheme 1. Illustration of the preparation of $MoS_2/TiSi_2$ via an in situ photo-assisted reduction method.

3. Experimental

3.1. Materials

Titanium disilicide was obtained from Alfa Aesar and all other chemicals (analytical purity) were obtained from J&K Scientific Limited (Beijing, China). All of the reagents and chemicals were utilized as received without further purification.

3.2. Synthesis

Fifty milliliters of 10 vol % lactic acid (LA) solution was added into to a 60 mL three-necked round-bottom flask with a quartz window, 50 mg of $TiSi_2$ and a certain amount of $(NH_4)_2MoS_4$ were dispersed in the lactic acid solution. The mixed solution was ventilated via bubbling argon with 30 min, then the mixture was irradiated by 150 W Xe lamp through the quartz window with a cutoff filter at 420 nm. After 60 min irradiation, the suspension was centrifuged and the solid was washed by ethanol first and then through deionized water. The obtained solid was dried under vacuum under 50 °C overnight, obtaining MoS_2 modified $TiSi_2$($MoS_2/TiSi_2$-x), where x represents the mass percentage of MoS_2 in the $MoS_2/TiSi_2$ composite. For comparison, MoS_2 was obtained in the same process without adding $TiSi_2$.

3.3. Characterization

X-Ray diffraction (XRD) measurement was performed under a Philips diffractometer (X'Pert-Pro MRD, Amsterdam, The Netherland) with a Ni-filtered Cu Kα source (λ = 0.15418 nm) in the 2θ scanning range from 10° to 90°. Scanning electron microscopy (SEM) was taken on SEM Hitachi S-4800 (Hitachi High-Tech, Tokyo, Japan). The energy-dispersive X-ray (EDX) was carried out in a KEVEX X-ray energy detector (KEVEX, Newark, NJ, USA). The transmission electron microscopy (TEM) was carried out by TECNAI-G2 electron microscope (FEI, Hillsboro, OR, USA) using 200 kV accelerating voltage. UV-vis absorption spectra (DRS) were performed on a Hitachi UV-3010 spectrophotometer (Hitachi High-Tech, Tokyo, Japan) with $BaSO_4$ as white standard. X-ray photoelectron spectroscopy (XPS) was determined on an AXIS Ultra DLD system (Kratos Analytical Inc., Manchester, UK) used a monochromatic Al Kα radiation and C 1s peak (285.5 eV) was as a reference to calibrate all of the XPS spectra using XPS Peak software (Version 4.1, Raymund W.M. Kwok, Hongkong, China).

3.4. Photoelectrochemical Measurements

All photoelectrochemical measurements were carried out in a three-electrode system connected with a CHI660D (CH Instruments Inc., Shanghai, China) electrochemical workstation. An indium tin oxide (ITO) glass covered by the sample was employed as the working electrode, a saturated calomel electrode (SCE) as the reference electrode and a platinum wire as the counter electrode. The working electrode was obtained first through dispersing 0.2 mg of the sample in 1 mL of a solution composed of 0.4 mL of ethanol, 0.4 mL of ethylene glycol and 0.2 mL of chloroform, after grinding and sonication, the slurry was then dropped onto a clean ITO glass and dried in vacuum at 45 °C. The sample area on the ITO glass was ca. 1.0 cm^2. During the photoelectrochemical measurements, the electrodes were immersed in 50 mL of 0.5 M Na_2SO_4 solution containing 5 mL lactic acid and the ITO glass with catalyst was irradiated by a GY-10 xenon lamp (150 W) (TIAN JIN TUO PU, Tianjin, China). Electrochemical impedance spectroscopy (EIS) was recorded under the frequency range 1–10^5 Hz with an AC perturbation signal of 5 mV.

3.5. Photocatalytic Reaction for Hydrogen Evolution

20 mg of as-prepared photocatalyst was added in 50 mL of 10 vol % lactic acid (LA) solution. The suspension was added into a 60 mL three-necked flask with quartz window. The area of the effective optical channel is ca. 3 cm^2. The reaction mixture was vigorously stirred and degassed via Ar with 30 min. Then the mixture was irradiated by 150 W Xe lamp through the quartz window with a cut-off filter at 420 nm. The lamp was positioned ca. 10 cm away from the optical entry window of the reactor. The distance between the lamp and the quartz window was ca. 10 cm. The gas chromatograph GC1650 (Ke Xiao Instruments Co., Ltd., Hangzhou, China) with a thermal conductivity detector (molecular sieve 5 A column, Ar carrier) was used to detected the amount of hydrogen production.

4. Conclusions

A robust and effective $MoS_2/TiSi_2$ photocatalyst has been successfully fabricated through the convenient in situ photo-reduction method. The characterization results of prepared catalysts reveal that the MoS_2 was evenly distributed at $TiSi_2$ forming heterojunctions benefiting photoexcited charges transfer and separation. The hydrogen production rate by the optimized $MoS_2/TiSi_2$ catalyst reaches 214.1 $\mu mol \cdot h^{-1} \cdot g^{-1}$ by visible light illumination, which is significantly superior to that of $TiSi_2$ and MoS_2. The characteristics possessed by $MoS_2/TiSi_2$, such as broad spectral response, enhanced absorption capability and the synergistic effect between MoS_2 and $TiSi_2$, are owed to high photocatalytic performance of the catalyst. This work demonstrates the feasibility of increasing H_2 evolution activity of $TiSi_2$-based catalysts by combining $TiSi_2$ with MoS_2.

Supplementary Materials: The following are available online at http://www.mdpi.com/2073-4344/9/3/299/s1, Figure S1: Morphology characterization of (A) $TiSi_2$ and (B) MoS_2 using SEM. Figure S2: EDX results of $MoS_2/TiSi_2$-3. Figure S3: A full-scan XPS of $TiSi_2$, MoS_2 and $MoS_2/TiSi_2$-3. Figure S4: The amount of H_2 evolved over the samples. Scheme S1: Schematic illustration of the catalytic mechanism.

Author Contributions: C.Z., Y.D. and P.Y. conceived and designed the experiments; C.Z., A.L. and K.L. performed the experiments; C.Z. and P.Y. analyzed the data and wrote the manuscript.

Funding: This research was funded by the National Natural Science Foundation of China (21373143).

Conflicts of Interest: None of the authors has any competing interests.

References

1. Chu, D.; Zhang, C.; Yang, P.; Du, Y.; Lu, C. WS_2 as an Effective Noble-Metal Free Cocatalyst Modified $TiSi_2$ for Enhanced Photocatalytic Hydrogen Evolution under Visible Light Irradiation. *Catalysts* **2016**, *6*, 136. [CrossRef]
2. Boyjoo, Y.; Sun, H.; Liu, J.; Pareek, V.K.; Wang, S. A review on photocatalysis for air treatment: From catalyst development to reactor design. *Chem. Eng. J.* **2017**, *310*, 537–559. [CrossRef]

3. Fujishima, A.; Honda, K. Electrochemical Photolysis of Water at a Semiconductor Electrode. *Nature* **1972**, *238*, 37–38. [CrossRef]
4. Zhao, H.; Wu, M.; Liu, J.; Deng, Z.; Li, Y.; Su, B.-L. Synergistic promotion of solar-driven H_2 generation by three-dimensionally ordered macroporous structured TiO_2-Au-CdS ternary photocatalyst. *Appl. Catal. B Environ.* **2016**, *184*, 182–190. [CrossRef]
5. Wen, J.; Li, X.; Li, H.; Ma, S.; He, K.; Xu, Y.; Fang, Y.; Liu, W.; Gao, Q. Enhanced visible-light H_2 evolution of g-C_3N_4 photocatalysts via the synergetic effect of amorphous NiS and cheap metal-free carbon black nanoparticles as co-catalysts. *Appl. Surf. Sci.* **2015**, *358 Pt A*, 204–212. [CrossRef]
6. Rajamanickam, D.; Dhatshanamurthi, P.; Shanthi, M. Enhanced photocatalytic efficiency of NiS/TiO_2 composite catalysts using sunset yellow, an azo dye under day light illumination. *Mater. Res. Bull.* **2015**, *61*, 439–447. [CrossRef]
7. Lin, Y.; Zhou, S.; Liu, X.; Sheehan, S.; Wang, D. TiO_2/$TiSi_2$ Heterostructures for High-Efficiency Photoelectrochemical H_2O Splitting. *J. Am. Chem. Soc.* **2009**, *131*, 2772–2773. [CrossRef] [PubMed]
8. Banerjee, S.; Mohapatra, S.K.; Misra, M. Water Photooxidation by $TiSi_2$–TiO_2 Nanotubes. *J. Phys. Chem. C* **2011**, *115*, 12643–12649. [CrossRef]
9. Pelleg, J.; Sade, G. TiB_2/$TiSi_2$ bilayer fabrication by various techniques: Structure and contact properties. *Phys. B Condens. Matter* **2006**, *371*, 20–34. [CrossRef]
10. Ritterskamp, P.; Kuklya, A.; Stkamp, M.-A.; Kerpen, K.; Weidenthaler, C.; Demuth, M. A Titanium Disilicide Derived Semiconducting Catalyst for Water Splitting under Solar Radiation—Reversible Storage of Oxygen and Hydrogen. *Angew. Chem. Int. Ed.* **2007**, *46*, 7770–7774. [CrossRef]
11. Shon, I.-J.; Park, H.-K.; Kim, H.-C.; Yoon, J.-K.; Hong, K.-T.; Ko, I.-Y. One-step synthesis and densification of nanostructured $TiSi_2$–SiC composite from mechanically activated (TiC + 3Si) powders by high-frequency-induced heated combustion. *Scr. Mater.* **2007**, *56*, 665–668. [CrossRef]
12. Liu, J.; Bai, Y.; Chen, P.; Cui, N.; Yin, H. Reaction synthesis of $TiSi_2$ and Ti_5Si_3 by ball-milling and shock loading and their photocatalytic activities. *J. Alloys Compd.* **2013**, *555*, 375–380. [CrossRef]
13. Mou, Z.; Yin, S.; Zhu, M.; Du, Y.; Wang, X.; Yang, P.; Zheng, J.; Lu, C. RuO_2/$TiSi_2$/graphene composite for enhanced photocatalytic hydrogen generation under visible light irradiation. *Phys. Chem. Chem. Phys.* **2013**, *15*, 2793–2799. [CrossRef]
14. Liu, Y.; Yu, Y.-X.; Zhang, W.-D. MoS_2/CdS Heterojunction with High Photoelectrochemical Activity for H_2 Evolution under Visible Light: The Role of MoS_2. *J. Phys. Chem. C* **2013**, *117*, 12949–12957. [CrossRef]
15. Chang, K.; Chen, W. In situ synthesis of MoS_2/graphene nanosheet composites with extraordinarily high electrochemical performance for lithium ion batteries. *Chem. Commun.* **2011**, *47*, 4252–4254. [CrossRef]
16. Nguyen, M.; Tran, P.D.; Pramana, S.S.; Lee, R.L.; Batabyal, S.K.; Mathews, N.; Wong, L.H.; Graetzel, M. In situ photo-assisted deposition of MoS_2 electrocatalyst onto zinc cadmium sulphide nanoparticle surfaces to construct an efficient photocatalyst for hydrogen generation. *Nanoscale* **2013**, *5*, 1479–1482. [CrossRef]
17. Lu, X.; Jin, Y.; Zhang, X.; Xu, G.; Wang, D.; Lv, J.; Zheng, Z.; Wu, Y. Controllable synthesis of graphitic C_3N_4/ultrathin MoS_2 nanosheet hybrid nanostructures with enhanced photocatalytic performance. *Dalton Trans.* **2016**, *45*, 15406–15414. [CrossRef]
18. Larciprete, R.; Danailov, M.; Barinov, A.; Gregoratti, L.; Kiskinova, M. Thermal and pulsed laser induced surface reactions in Ti/Si(001) interfaces studied by spectromicroscopy with synchrotron radiation. *J. Appl. Phys.* **2001**, *90*, 4361–4369. [CrossRef]
19. Fouad, O.A.; Yamazato, M.; Era, M.; Nagano, M.; Hirai, T.; Usui, I. Preparation and properties of $TiSi_2$ thin films from $TiCl_4$/H_2 by plasma enhanced chemical vapor deposition. *J. Cryst. Growth* **2002**, *234*, 440–446. [CrossRef]
20. Wee, A.T.S.; Huan, A.C.H.; Osipowicz, T.; Lee, K.K.; Thian, W.H.; Tan, K.L.; Hogan, R. Surface and interface studies of titanium silicide formation. *Thin Solid Films* **1996**, *283*, 130–134. [CrossRef]
21. Zong, X.; Yan, H.; Wu, G.; Ma, G.; Wen, F.; Wang, L.; Li, C. Enhancement of Photocatalytic H_2 Evolution on CdS by Loading MoS_2 as Cocatalyst under Visible Light Irradiation. *J. Am. Chem. Soc.* **2008**, *130*, 7176–7177. [CrossRef]
22. Yue, Z.; Chu, D.; Huang, H.; Huang, J.; Yang, P.; Du, Y.; Zhu, M.; Lu, C. A novel heterogeneous hybrid by incorporation of Nb_2O_5 microspheres and reduced graphene oxide for photocatalytic H_2 evolution under visible light irradiation. *RSC Adv.* **2015**, *5*, 47117–47124. [CrossRef]

23. Franceschini, E.A.; Gomez, M.J.; Lacconi, G.I. One step synthesis of high efficiency nickel/mesoporous TiO_2 hybrid catalyst for hydrogen evolution reaction. *J. Energy Chem.* **2019**, *29*, 79–87. [CrossRef]
24. Bahrami, A.; Kazeminezhad, I.; Abdi, Y. Pt-Ni/rGO counter electrode: Electrocatalytic activity for dye-sensitized solar cell. *Superlattices Microstruct.* **2019**, *125*, 125–137. [CrossRef]
25. Li, Y.; Zhang, H.-X.; Liu, F.-T.; Dong, X.-F.; Li, X.; Wang, C.-W. New design of oriented NiS nanoflower arrays as platinum-free counter electrode for high-efficient dye-sensitized solar cells. *Superlattices Microstruct.* **2019**, *125*, 66–71. [CrossRef]
26. Vishnu, N.; Badhulika, S. Single step grown MoS_2 on pencil graphite as an electrochemical sensor for guanine and adenine: A novel and low cost electrode for DNA studies. *Biosens. Bioelectron.* **2019**, *124*, 122–128. [CrossRef] [PubMed]